Nanoscale

Accepted Manuscript

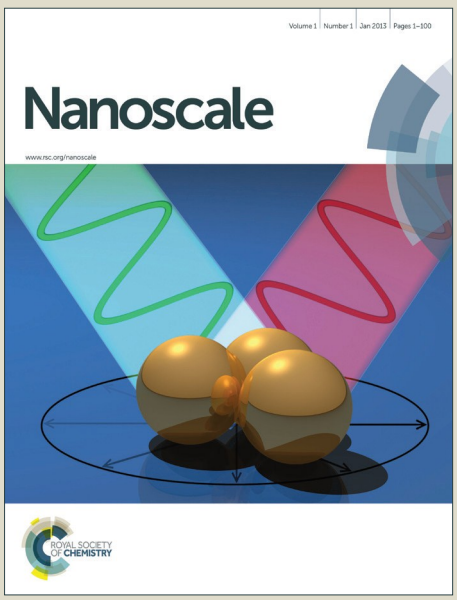

This is an *Accepted Manuscript*, which has been through the Royal Society of Chemistry peer review process and has been accepted for publication.

Accepted Manuscripts are published online shortly after acceptance, before technical editing, formatting and proof reading. Using this free service, authors can make their results available to the community, in citable form, before we publish the edited article. We will replace this *Accepted Manuscript* with the edited and formatted *Advance Article* as soon as it is available.

You can find more information about *Accepted Manuscripts* in the Information for Authors.

Please note that technical editing may introduce minor changes to the text and/or graphics, which may alter content. The journal's standard Terms & Conditions and the Ethical guidelines still apply. In no event shall the Royal Society of Chemistry be held responsible for any errors or omissions in this *Accepted Manuscript* or any consequences arising from the use of any information it contains.

ROYAL SOCIETY OF CHEMISTRY

www.rsc.org/nanoscale

Please do not adjust margins

Journal Name

ARTICLE

A highly efficient thermo-optic microring modulator assisted by graphene

Received 00th January 20xx,
Accepted 00th January 20xx

DOI: 10.1039/x0xx00000x

www.rsc.org/

Sheng Gan[1], Chuantong Cheng[2], Yaohui Zhan[3], Beiju Huang[2], Xuetao Gan[4], Shaojuan Li[1], Xiaofeng Li[3], Jianlin Zhao[4], Hongda Chen[2,*] and Qiaoliang Bao[1,5,*]

Graphene's remarkable electrical and optical properties afford great potential for constructing various optoelectronic devices, including modulators, photodetectors and pulse lasers. In particular, graphene-based optical modulators were demonstrated to be featured with broadband response, small footprint, ultrafast speed and CMOS-compatibility, which may provide an alternative architecture for light-modulation in integrated photonic circuits. While on-chip graphene modulators have been studied in various structures, most of them are based on capacitance-like configuration subjected to complicated fabrication processes and a low yield of working devices. Here, we experimentally demonstrate a new type of graphene modulator by employing graphene's electrical and thermal properties, which can be achieved with a simple fabrication flow. On a graphene-coated microring resonator with a small active area of 10 μm^2, we have obtained an effective optical modulation via thermal energy electrically generated in graphene layer. The resonant wavelength of the ring resonator shifts 2.9 nm under an electrical power of 28 mW, which enables a large modulation depth of 7 dB and a broad operating wavelength range of 6.2 nm with 3 dB modulation. Due to extremely high electrical and thermal conductivity in graphene, the graphene thermo-optical modulator operates at a very fast switching rate compared with the conventional silicon thermo-optic modulator, i.e., 10% - 90% rise (90% - 10% fall) time of 750 ns (800 ns). The results promise a novel architecture for massive on-chip modulation of optical interconnects compatible with CMOS technology.

1. Introduction

Optical interconnects constructed on silicon processing chips have been investigated widely due to the compact footprint, low energy consumption and compatibility with on-chip electrical links. Although silicon is excellent for passive optical components such as waveguides and filters, it is challenging to achieve high-performance optical modulation using pure silicon material due to its low electro-optic coefficient and low carrier mobility. Consequently, silicon modulators were subjected to issues of large device size, thermal instabilities and complicated fabrication processes[1-6]. Improved modulators which integrate new active materials onto the silicon chip to realize large extinction ratio, small footprint and low-power consumption are highly desired.

Graphene, the most-renowned two-dimensional material, has been extensively investigated in optoelectronics due to its excellent electrical and optical properties[7-9]. Specifically, graphene's linear dispersion of the Dirac fermions, ultrafast carrier mobility and strong interaction with light open a door for high-

1 Institute of Functional Nano and Soft Materials (FUNSOM), Jiangsu Key Laboratory for Carbon-Based Functional Materials and Devices, and Collaborative Innovation Center of Suzhou Nano Science and Technology, Soochow University, Suzhou 215123, P. R. China
2 State Key Laboratory on Integrated Optoelectronics, Institute of Semiconductors, Chinese Academy of Sciences, Beijing 100083, China
3 College of Physics, Optoelectronics and Energy & Collaborative Innovation Center of Nano Science and Technology, Soochow University, Suzhou 215006, China
4 Key Laboratory of Space Applied Physics and Chemistry, Ministry of Education, and Shaanxi Key Laboratory of Optical Information Technology, School of Science, Northwestern Polytechnical University, Xi'an 710072, China
5 Department of Materials Science and Engineering, Monash University, Clayton, Victoria 3800, Australia

Nanoscale Accepted Manuscript

Please do not adjust margins

performance optoelectronic devices such as optical modulators,[10-15] photodetectors,[16-21] polarizers[22] and saturable absorbers[23,24]. Graphene's carrier concentration varies significantly upon external electric field or chemical doping, which will shift the Fermi level and subsequently tune the absorption strength. Based on this electro-optic effect, graphene has been integrated into a photonic crystal nanocavity[15] or waveguide structures[10-14] for ultrafast or broadband light modulation. However, most of these devices have a capacitance-like configuration and suffer from a relatively lengthy fabrication flow as well as a low yield of workable devices, which significantly restrict the application for massive optical interconnects. In addition, the existing ring optical modulators based on graphene either suffer from a low modulation depth[12] or a large device footprint[14].

Practically, thermo-optic modulator could be a more feasible solution considering the large thermo-optic coefficient (1.86×10^{-4} K^{-1}) in silicon and intensive researches in the last decades.[25-29] It is noteworthy that the thermal conductivity of graphene is as high as 5300 W $(mK)^{-1}$,[30] which is ~100 times higher than that of gallium aesnide,[31] indicating an excellent capability of transferring heat at a high speed. It has been reported that graphene can induce a fast temperature variation of about 100 °C when injected by 12 mW electrical power.[32] To this point, the combination of graphene with silicon chip for thermo-optic modulation will synergistically marry the Joule heating effect and ultrahigh thermal conductivity in graphene with the thermo-optical effect in silicon. Due to the simple fabrication of an electrically actuated graphene heater and conductor on silicon structure, the graphene-assisted thermo-optic modulator could become an alternative for capacitance-based modulators. Furthermore, the layered nature of graphene and its flexibility enable good compatibility with CMOS-technology.

In this article, we report a highly efficient thermo-optic modulator consisting of monolayer graphene on a silicon microring resonator. Because of the ultra-narrow resonant peaks and small mode volume, silicon microring resonators have been widely studied in optical modulators,[33,34] filters[35-37] and sensors[38,39]. It is well known that a minor variation of effective refractive index in the ring resonator, induced by carrier plasma effect or thermal effect, would shift the resonant peaks or change their intensities significantly. Hence, with the incorporation of an effective graphene heater, a microring thermo-optic modulator is expected to deliver high extinction ratio and low-power consumption. Due to the efficient modification of the effective index via graphene heating, a resonant wavelength shift of 2.7 nm and a modulation depth up to 7 dB have been demonstrated with the electrical power of 28 mW in the graphene/silicon thermo-optic modulator. Compared with the state-of-the-art of silicon based thermo-optic ring modulators, the operation power and modulation depth fall almost the same level. More importantly, the response speed is improved from typical micro-seconds to nano-seconds. In principle, the proposed device has the potential for operation at tens of megahertz providing that the contact resistance is suppressed more effectively. It provides a simple method to fabricate the thermo-optic modulators and can find applications in wavelength filter or switching arrays.

2. Results and discussion

2.1. Structure design and device fabrication

The schematic of the microring thermo-optic modulator assisted by graphene is illustrated in Figure 1a. A single straight waveguide is coupled to a race-track ring resonator, which are covered by the monolayer graphene. Electrical signals are applied on graphene by two electrodes to produce Joule heating. The heat is transferred onto the microring and therefore causes change in the real and imaginary parts of refractive index due to the thermal effect on lattice and carrier. Consequently, the resonant wavelength and strength will be tuned.[40]

Nanoscale Accepted Manuscript

This journal is © The Royal Society of Chemistry 2015

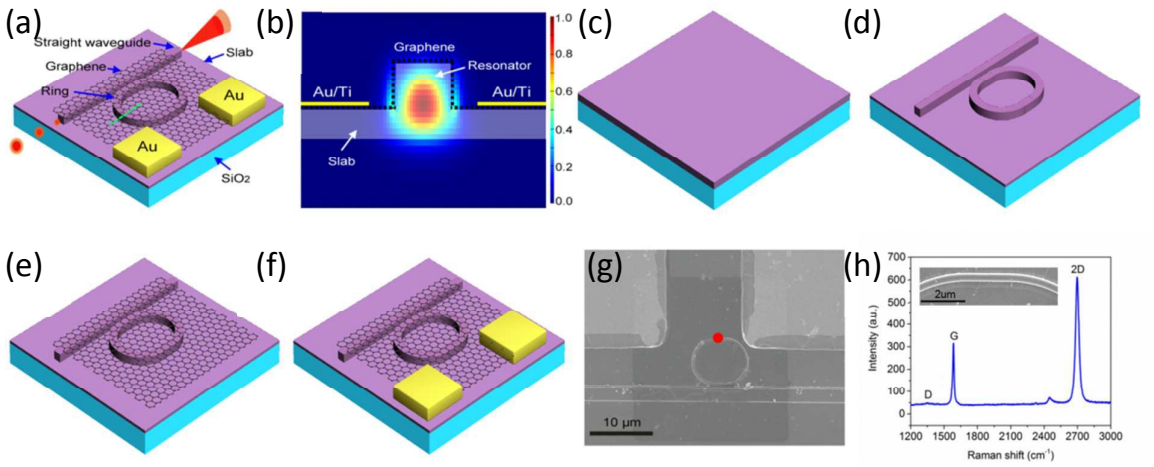

Figure 1 A thermo-optic microring modulator based on graphene. (a) Three dimensional illustration of thermo-optic microring modulator based on graphene; monolayer graphene is on top of ring resonator without any separation layer. (b) Cross-sectional diagram with the distribution of optical field superimposed over the waveguide. It corresponds to the green dash line in (a) and voltage is applied to both electrodes. (c) The device begins from a SOI wafer with 340 nm silicon on top and 1 μm buried oxide layer. (d) EBL and ICP etching were sequentially performed to fabricate the waveguide on the wafer. (e) Wet-transfer of CVD graphene onto microring. The active region was defined by lithography and O_2 plasma etching. (f) Deposition of Au/Ti electrodes. (g) SEM image showing detailed structure of a complete device. The square shape dark region refers to monolayer graphene film. (h) Raman spectrum and amplified SEM image of monolayer graphene taken at the position of the red dot in panel (g).

In order to approach the critical coupling[40] at the presence of graphene, we designed the resonator by optimizing the geometry based on finite difference time domain (FDTD) simulation. The key parameters controlling the resonance include the radius of microring, gap between microring and straight waveguide, and height of the waveguide. The aim is to obtain a large extinction ratio at desired wavelength in microring. Considering the fact that graphene on waveguide has large absorption of transverse magnetic (TM) mode,[10] we choose transverse electric (TE) mode as guiding mode which also has many other benefits such as lower insertion loss and higher coupling efficiency. The selection of TE mode enhanced the device compatibility in terms of on-chip integration with the laser-diode architecture, which typically emits in the TE polarization due to smaller lasing threshold. The optical guiding mode in the graphene-silicon hybrid waveguide was simulated, as shown in Figure 1b. It was found that the optical field is dominantly concentrated in central part of the waveguide, thus minimizing the optical loss caused by graphene film on top of the waveguide. In addition, to avoid the mode leakage, both electrodes are located more than 1 μm away from the resonator.

The detailed device process is schematically illustrated in Figures 1c-f. We fabricated the microring modulator on a silicon-on-insulator (SOI) wafer with 340 nm thick top silicon layer and a 1 μm thick buried oxide layer. Both the straight and ring waveguide have a width of 400 nm and a height of 220 nm with the gap between them as 100 nm. The bending radius of the ring is 3.4 μm and the length of straight section is 1.96 μm. These are optimized parameters for coupling more light into microring so as to achieve large extinction ratio in such a small footprint. A pair of tapered gratings was designed at both ends of the straight waveguide for efficient coupling of TE mode. All these structures were defined by electron beam lithography (EBL) and fabricated by inductively coupled plasma (ICP) etching. A large size graphene sheet prepared on copper film by

Nanoscale Accepted Manuscript

chemical vapor deposition (CVD), was transferred onto the silicon waveguide using the standard wet-transfer technique.[41] Photo-lithography was subsequently applied to define the active region and O_2 plasma was employed to remove the undesired graphene. Finally, both electrodes (Au/Ti: 100/10 nm) were deposited following the second-time photo-lithography. Figure 1g shows the top-view scanning electron microscopy (SEM) image of a fabricated device. The Raman spectrum (Figure 1h) of graphene on the device shows three characteristic peaks, *i.e.*, D band at 1343 cm^{-1}, G band at 1585 cm^{-1}, and 2D band at 2697 cm^{-1}. The intensity ratio of 2D/G is as large as 4, indicating the monolayer nature of graphene sample. The almost invisible D band, together with the amplified SEM image, suggests high quality of the graphene film even after multiple fabrication procedures.

2.2. Static electro-optical response of the device

We first investigated the static electro-optical response of our device using a continuous-wave broadband light source (1520~1580 nm). The averaged coupling efficiency is found to be 22 dB for both input and output couplers. Figure 2a depicts the normalized transmission spectra around the resonant wavelength of λ_0 = 1554.9 nm while applying different voltages. Without the external bias, the resonance shows a 9.6 dB drop of the transmission with a 3 dB bandwidth of 4.6 nm, as indicated by the black line. Such a low transmission at the resonant wavelength is considered as the "OFF" state of the ring modulator. While applying a bias, the resonant notch was red-shifted, resulting in the variation of transmission at the resonant wavelength. At the maximum bias of 7 V, the transmission drop of the resonance rise to a value of 2.6 dB, which is the "ON" state of the ring modulator.

Figure 2b illustrates the changes of the resonant wavelength and quality (Q) factor as a function of the applied voltage. It is found that 2.9 nm shift is achieved while the bias voltage is increased from 0 V to 7 V, which corresponds to 28 mW electrical power injection. As a result, an efficiency of 9.7 mW/nm is obtained, which is quite small compared with conventional silicon thermo-optical resonator.[25-28] The Q factor of resonance is described by $Q = 4\pi^2 n_g R/\lambda_0 \kappa^2$, where κ is the coupling coefficient between the straight waveguide and the ring resonator, and n_g is the group index of the ring hybrids. It is noted that the Q factor decreases from 338 to 227 with the increase in the bias voltage. This can be attributed to resonant wavelength shift of silicon microring. We also note that the notch depth of the resonance becomes shallow at larger bias, which is the consequence of extra absorption loss induced by thermal-excited carriers[42].

The blue trace in Figure 2c depicts the transfer function of the modulator at the wavelength of 1554.9 nm. It is revealed that the transmission increases exponentially with the increment of bias voltage. The resonance of this device can completely detune from the probe wavelength, thereby forming a modulation from "0" to "1". It should be noted that a modulation of 68% (5 dB) can be obtained with a voltage variation of merely 2 V, namely from 5 V to 7 V, which is of fairly high efficiency in graphene-based optical modulator. Figure 2c also plots the linear relationship between the electric current and the applied voltage. The total resistance between the two electrodes is calculated to be 1920 Ω. The sheet resistance of our square-shaped graphene sample is in the range of 350 to 500 Ω/□, which indicates that the contact resistance is about 1500 Ω. One can reduce the contact resistance using noble metal as the adhesion layer between gold electrode and graphene, thus concentrating more heat into the ring part subsequently leading to higher modulation efficiency. Note that the relatively low Q factor of the resonant mode in the graphene-integrated ring promises a broadband operation of the modulator, as shown in Figure 2d, which was obtained by comparing the transmission spectra under the voltages of 0 V and 7 V. We achieved the modulation depth larger than 3 dB over a broad range of 6.2 nm, namely from 1552.7 nm to 1555.8 nm and from 1556.8 nm to 1559.9 nm, in which the largest depth can reach as high as 7dB (80%).

2.3. Numerical simulation

We then performed analytical explanations on the above static electro-optical response. As the voltage increases, the current flow causes Joule heating which will be further transferred to underlying silicon and result in the variation of refractive index. The change of refractive

Nanoscale Accepted Manuscript

This journal is © The Royal Society of Chemistry 2015

index can be fitted with $dn/dT = 1.86\times10^{-4}$ /K, where n is the real part of the index and T is temperature in Kelvin. Besides, the transferred heat in the cavity will also cause the increment of electron-hole pairs leading to the variation of both real and imaginary (*i.e.,* optical absorption) parts of its refractivity according to plasma dispersion effect. The change in real part of the refractivity normally manifests as the shift of the transmission spectrum, whereas the change of imaginary part will modify the extinction ratio because the imaginary part is related to optical loss. Specifically, the increase of temperature will change the real part of the refractivity by ~10^{-2} via the thermo-optic effect. However, the increase of free carriers (~10^{11} cm^{-3})[42] causes negligibly small reduction (~10^{-8}) of the real part of the refractivity and a moderate variation of the imaginary part (~10^{-6}) of the refractivity.

To quantitatively study the changes of resonant wavelength (λ_0) and the extinction ratio as a function of bias voltage, the classical photonic circuit model was used. The transmitted power at resonance versus ring transmission α can be described by[40]

$$T(\lambda_0) = \frac{(\alpha - |t|)^2}{(1-\alpha|t|)^2} \quad (1)$$

where α = exp $(-\tau \bullet L)$, τ is the optical absorption coefficient of the cavity with a circumference of L, t is the single-pass transmission through the straight waveguide adjacent to the ring which is a constant value with a specific structure. On the basis of critical coupling conditions of the ring resonator, the extinction ratio will decrease due to the extra optical absorption induced by thermal-excited carriers in under-coupled condition. This is the main reason responsible for up-shift of the transmission dip observed in Figure 2a.

The dependence of the resonant wavelength shift on effective refractive index is expressed by the formula[29]

$$\partial\lambda = \frac{\lambda \Delta N_{eff}}{N_{ring.eff}} \quad (2)$$

where $\Delta N_{eff,ring} \approx (dn/dT)\Delta T$, $N_{eff,ring}$ and λ are real part of the effective index and resonant wavelength, respectively. According to the above discussion, the increase of effective index $N_{eff,ring}$ is proportional to the temperature of ring waveguide. That is why the transmission spectrum red-shifts upon the heating of

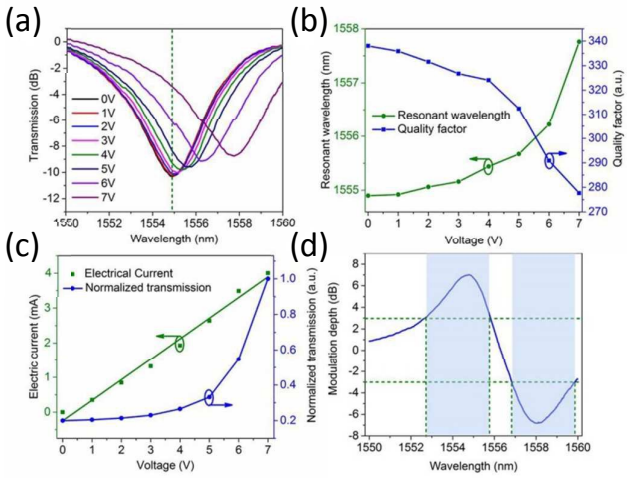

Figure 2 Static thermo-optic response of the ring modulator. (a) The main panel shows the transmission spectra of the ring resonator at different drive voltages; the vertical olive dashed line indicates the location of the resonant wavelength which is employed in dynamic response measurement and transfer function at 1554.9 nm. (b) The changes of the resonant wavelength and Q factor as a function of the applied voltage. (c) The electric current of the circuit and the normalized transmissions of the waveguide at 1554.9 nm versus the applied voltage; the olive green line shows a linear fit to the experimental data which yields the contact resistance of about 1500 Ω between graphene and the electrodes. (d) The modulation depth at different wavelengths obtained by comparing the transmission spectra under the voltages of 0 V and 7 V; the vertical olive dashed lines indicate the wavelength range of 6.2 nm over which modulation depth larger than 3 dB is achieved.

graphene. In comparison, the change of refractive index or absorption in graphene at high temperature is relatively small, which only causes a negligible shift of resonant mode of the ring cavity. At the probe wavelength (λ_0=1554.9 nm), 7 dB modulation and 2.9 nm shift were observed. Based on FDTD simulation, $N_{eff,ring}$=2.8067, and $\Delta N_{eff,ring}$ is found to be ~0.0056. As a result, we can conclude that $\Delta T \approx 30$ K is caused by the Joule heating of graphene.

In order to verify the Joule heating effect by graphene, a numerical model was built to simulate the

Nanoscale Accepted Manuscript

temperature distribution of the resonator device, as shown in Figure 3a, 3b.With the injection electrical power of 28 mW, the maximal temperature in graphene can reach as high as 75 °C in the central part of the ring resonator where graphene is suspended. In other region, graphene forms a close contact with the underlying silicon waveguide and the heat will be instantly transferred to silicon microring at high speed and efficiency. Consequently, a temperature variation up to 33 °C is observed (Figure 3b), which is in good agreement with experimental results ($\Delta T \approx 30$ K). The temperature change of the ring would subsequently induce a change of refractive index via the thermo-optic effect and variation of silicon carrier density,[42] which are responsible for large shift of resonant wavelength and decreased extinction ratio.

It is interesting to find that the temperature in the hottest point of the ring resonator is exponentially promoted with the increase of applied voltage, as shown in Figure 3c. This trend is generally consistent with that of resonant wavelength shift versus applied voltage (Figure 2b). Figure 3d depicts the transient heat-up process of graphene, where the temperature is taken from the point indicated by blue dot in Figure 3a. It is revealed that the heating time for reaching a stable temperature is less than 100 ns, which indicates the fast dynamic response of the thermo-optic modulator.

It is also noticed that there is an overshoot at 5 ns before the temperature is slightly reduced and eventually stabilized after 66 ns (Figure 3d). The overshoot is induced by the rate difference of heat production and transfer. At first, the temperature increase in graphene is so fast that the heat is not transferred away in time, resulting in the largest temperature difference between graphene heater and underlying silicon. Following, most of the heat is transferred after 5 ns and the temperature begins to drop. As the temperature difference reduces, the amount of transferred heat decreases, thus leading to a slow temperature increase in graphene. Finally, the heat conduction is stabilized and the temperature difference becomes zero.

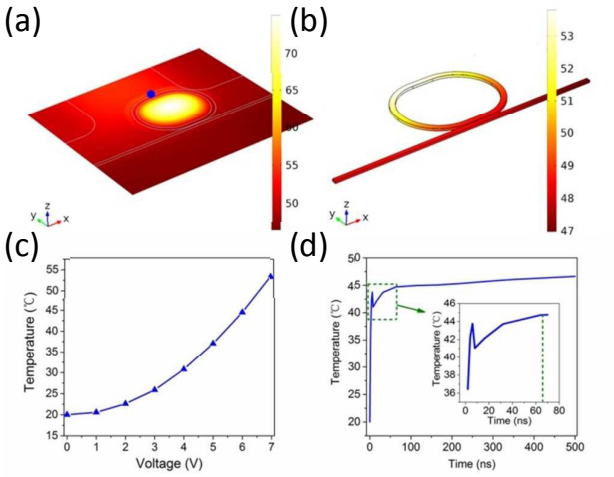

Figure 3 Simulation of the device using COMSOL. (a) Temperature increase of graphene when 28 mW electrical power was injected. (b) Corresponding thermal distribution of the ring resonator induced by graphene heater. (c) Simulated temperature variation monitored at the hottest position of the ring resonator under different drive voltages. (d) Temporal behavior of the graphene heater taken at the position of the blue dot in figure (a); the inset shows the enlarged view of the overshoot.

2.4. Dynamic electro-optical response of the device

To measure the dynamic response of the modulator, electrical signal output by an arbitrary waveform generator with a static voltage was applied to the device. Figures 4a, 4b show the waveforms of the normalized optical output at 200 KHz and 300 KHz, respectively. The peak-to-peak voltage of the driving signal is 6 V (from 1 V to 7 V). According to the 10% -90% rule, the rise and fall time were measured as 750 ns and 800 ns, respectively. This is nearly at the same magnitude of order of that deduced by the theoretical prediction in Figure 3d. The rise and fall times are in the range of nanoseconds, which is faster than silicon-based thermo-optic modulators[25-28]. Such a high modulation speed is attributed to superior thermal conductivity and fast heat generation of graphene.

Nanoscale Accepted Manuscript

This journal is © The Royal Society of Chemistry 2015

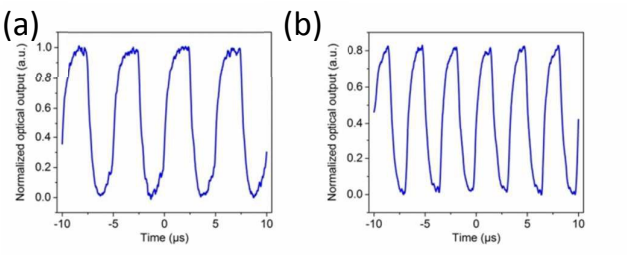

Figure 4 Dynamic response of the device. (a) Waveform of the optical output of the device at 200 KHz; the data was normalized to the output power at the drive voltage of 7 V. (b) Waveform of the normalized optical output of the device at 300 KHz; the 10% - 90% rise time and 90% - 10% fall time are measured to be 750 ns and 800 ns, respectively. The result is nearly at the same magnitude of the order of the theoretical prediction.

In our device, graphene lying on the ring resonator acts as both heater and heat conductor. The cut-off frequency f of the thermal response is limited by many factors including heating area A, switching power P, specific heat C_p and density ρ of the heater according to the relationship $f \propto P/(A \bullet \rho \bullet C_p)$.[43] It also provides some clues for developing even faster device with larger extinction ratio by optimizing the structure design and electrode location. Moreover, the specific heat and the density of the heater are expected to decrease if even higher quality graphene is used. Hence, this type of device is very likely to operate at even tens of megahertz for a faster thermo-optic modulation, which is also predicted by the aforementioned simulation results.

3. Conclusion

In conclusion, we have demonstrated a graphene-based thermo-optic modulator on silicon microring resonator. A large shift of the transmission spectrum is achieved with a low electrical power injection. The device has a high modulation depth of 7 dB in a small footprint of 10 μm^2. A broadband modulation with bandwidth of 6.2 nm was observed. Both experimental and theoretical results indicate that its operation speed promises to be as large as tens of megahertz which is the fastest in the field of thermo-optic modulation to date. Its active area of merely tens of square microns can be further reduced to suit for massive on-chip optical interconnects, which will have great potential for development of optical communications, sensing and imaging. Furthermore, the property of selectively modulating wavelength is suitable for constructing wavelength division multiplexing so that the bandwidth of the optical interconnects can be improved significantly.

4. Experimental section

We characterized the fabricated device at room temperature in ambient conditions. A continuous-wave light from a broadband light source (Hoyatek, ASE) was coupled to the device and the output spectra were measured by an optical spectrum analyzer (Agilent, 86145B). Drive voltage was applied by a triple output DC power supply (Agilent, E3681A) and tuned by an arbitrary waveform generator (Agilent, 33250A). A tunable laser source (Southern Photonics, TLS150D) was used as input for the characterization of dynamic response. The dynamic optical output of the device was directed into an infrared photoreceiver (Newport, Model 1544, 12 GHz) with the waveform recorded on a mixed signal oscilloscope (Agilent, MSO-X 3034A, 350 MHz).

The thermal processes including Joule heating by graphene, convective heat transfer and temperature variation in microring resonator were numerically simulated by finite element method (FEM) using COMSOL. In particular, the temperature of interest region under different drive voltages as well as the transient temperature increment was calculated to verify the experimental observations. An extra fine free triangular mesh was used for graphene film (thickness: 0.35 nm) to achieve more reliable results. It was assumed that graphene layer has a uniform heat flux and the convective heat transfer was imposed on the top of the device. Specifically, the heat transfer coefficient h is set to be 10 $Wm^{-2}K^{-1}$ with initial temperature of T_0 = 20 ℃. The electrical conductivity of graphene is 2×10^5 S m^{-1}.[44] The thermal conductivities of graphene[45] and silicon are set as 4000 W $(mK)^{-1}$ and 148 W $(mK)^{-1}$,

Nanoscale Accepted Manuscript

respectively. The specific heat of graphene is 2082 J $(kgK)^{-1}$ and the specific heat of silicon is 700 J $(kgK)^{-1}$.

Acknowledgments

We acknowledge the support from the National High Technology Research and Development Program of China (863 Program) (Grant No. 2013AA031903), the youth 973 program (2015CB932700), the National Natural Science Foundation of China (Grant No. 51222208, 51290273, 91433107, 61178051, 61321063), the Doctoral Fund of Ministry of Education of China (Grant No. 20123201120026), ARC DECRA (DE120101569), DP (DP140101501). This work was performed in part at the Melbourne Centre for Nanofabrication (MCN) in the Victorian Node of the Australian National Fabrication Facility (A3NFF). S. Li acknowledges the support from the Natural Science Foundation of Jiangsu Province (No. BK20130328), China Postdoctoral Science Foundation (No.2014M551654) and Jiangsu Province Postdoctoral Science Foundation (No. 1301020A).

References

1 G. T. Reed, G. Mashanovich, F. Y. Gardes, D. J. Thomson, *Nat. Photon.* 2010, **4**, 518.
2 A. Liu, R. Jones, L. Liao, D. Samara-Rubio, D. Rubin, O. Cohen, R. Nicolaescu, M. Paniccia, *Nature* 2004, **427,** 615.
3 Q. Xu, B. Schmidt, S. Pradhan, M. Lipson, *Nature* 2005, **435**, 325.
4 W. M. Green, M. J. Rooks, L. Sekaric, Y. A. Vlasov, *Opt. Express* 2007, **15**, 17106.
5 L. Zhang, Y. C. Li, J. Y. Yang, M. P. Song, R. G. Beausoleil, A. E. Willner, *IEEE J. Sel. Top. Quant.* 2010, **16**, 149.
6 D. M. Gill, M. Rasras, K. Y. Tu, Y. K. Chen, A. E. White, S. S. Patel, D. Carothers, A. Pomerene, R. Kamocsai, C. Hill, J. Beattie, *IEEE Photon. Tech. Lett.* 2009, **21**, 200.
7 K. S. Novoselov, A. K. Geim, S. V. Morozov, D. Jiang, Y. Zhang, S. V. Dubonos, I. V. Grigorieva, A. A. Firsov, *Science* 2004, **306**, 666.
8 A. K. Geim, K. S. Novoselov, *Nat. Mater.* 2007, **6**, 183.
9 L. Liao, Y.-C. Lin, M. Bao, R. Cheng, J. Bai, Y. Liu, Y. Qu, K. L. Wang, Y. Huang, X. Duan, *Nature* 2010, **467**, 305.
10 M. Liu, X. Yin, E. Ulin-Avila, B. Geng, T. Zentgraf, L. Ju, F. Wang, X. Zhang, *Nature* 2011, **474**, 64.
11 M. Liu, X. B. Yin, X. Zhang, *Nano Lett.* 2012, **12**, 1482.
12 C. Qiu, W. Gao, R. Vajtai, P. M. Ajayan, J. Kono, Q. Xu, *Nano Lett.* 2014, **14**, 6811.
13 N. Youngblood, Y. Anugrah, R. Ma, S. J. Koester, M. Li, *Nano Lett.* 2014, **14**, 2741.
14 T. P. Christopher, D. L. Yoon-Ho, C. Jaime, L. Michal, *Nature Photon.* 2015, **9**, 122.
15 X. T. Gan, R. J. Shiue, Y. D. Gao, K. F. Mak, X. W. Yao, L. Z. Li, A. Szep, D. Walker, J. Hone, T. F. Heinz, D. Englund, *Nano Lett.* 2013, **13**, 691.
16 T. Mueller, F. Xia, P. Avouris, *Nat. Photon.* 2010, **4**, 297.
17 F. Xia, T. Mueller, Y.-m. Lin, A. Valdes-Garcia, P. Avouris, *Nat Nanotechnol.* 2009, **4**, 839.
18 M. Furchi, A. Urich, A. Pospischil, G. Lilley, K. Unterrainer, H. Detz, P. Klang, A. M. Andrews, W. Schrenk, G. Strasser, T. Mueller, *Nano Lett.* 2012, **12**, 2773.
19 X. T. Gan, R. J. Shiue, Y. D. Gao, I. Meric, T. F. Heinz, K. Shepard, J. Hone, S. Assefa, D. Englund, *Nat. Photon.* 2013, 7, 883.
20 A. Pospischil, M. Humer, M. M. Furchi, D. Bachmann, R. Guider, T. Fromherz, T. Mueller, *Nat. Photon.* 2013**,** 7, 892.
21 X. M. Wang, Z. Z. Cheng, K. Xu, H. K. Tsang, J. B. Xu, *Nat. Photon.* 2013, **7,** 888.
22 Q. L. Bao, H. Zhang, B. Wang, Z. H. Ni, C. H. Y. X. Lim, Y. Wang, D. Y. Tang, K. P. Loh, *Nat. Photon.* 2011, **5**, 411.
23 Q. L. Bao, H. Zhang, Y. Wang, Z. H. Ni, Y. L. Yan, Z. X. Shen, K. P. Loh, D. Y. Tang, *Adv. Funct. Mater.* 2009, **19,** 3077.

Nanoscale Accepted Manuscript

This journal is © The Royal Society of Chemistry 2015

24 Z. P. Sun, T. Hasan, F. Torrisi, D. Popa, G. Privitera, F. Q. Wang, F. Bonaccorso, D. M. Basko, A. C. Ferrari, *ACS Nano* 2010, **4**, 803.
25 M. Nedeljkovic, S. Stankovic, C. J. Mitchell, A. Z. Khokhar, S. A. Reynolds, D. J. Thomson, F. Y. Gardes, C. G. Littlejohns, G. T. Reed, G. Z. Mashanovich, *IEEE Photon. Technol. Lett.* 2014, **26**, 1352.
26 A. Densmore, S. Janz, R. B. Ma, J. H. Schmid, D. X. Xu, A. Delage, J. Lapointe, M. Vachon, P. Cheben, *Opt. Express* 2009, **17**, 1047.
27 F. Gan, T. Barwicz, M. A. Popovic, M. S. Dahlem, C. W. Holzwarth, P. T. Rakich, H. I. Smith, E. P. Ippen, F. X. Kartner, *Photon. in Switching* 2007, **67**.
28 P. Dong, W. Qian, H. Liang, R. Shafiiha, D. Z. Feng, G. L. Li, J. E. Cunningham, A. V. Krishnamoorthy, M. Asghari, *Opt. Express* 2010, **18**, 20298.
29 P. Dong, R. Shafiiha, S. Liao, H. Liang, N.-N. Feng, D. Feng, G. Li, X. Zheng, A. V. Krishnamoorthy, M. Asghari, *Opt. Express* 2010, **18**, 10941.
30 A. A. Balandin, S. Ghosh, W. Bao, I. Calizo, D. Teweldebrhan, F. Miao, C. N. Lau, *Nano Lett.* 2008, **8**, 902.
31 Q. Bao, K. P. Loh, *ACS Nano* 2012, **6**, 3677.
32 J. T. Kim, K. H. Chung, C.-G. Choi, *Opt. Express* 2013, **21**, 15280.
33 Q. Xu, S. Manipatruni, B. Schmidt, J. Shakya, M. Lipson, *Opt. Express* 2007, **15**, 430.
34 Q. Xu, B. Schmidt, S. Pradhan, M. Lipson, *Nature* 2005, **435**, 325.
35 M. S. Rasras, K. Y. Tu, D. M. Gill, Y. K. Chen, A. E. White, S. S. Patel, A. Pomerene, D. Carothers, J. Beattie, M. Beals, J. Michel, L. C. Kimerling, *J. Lightwave Technol.* 2009, **27**, 2105.
36 H. Shen, M. H. Khan, L. Fan, L. Zhao, Y. Xuan, J. Ouyang, L. T. Varghese, M. H. Qi, *Opt. Express* 2010, **18**, 18067.
37 Q. Li, S. Yegnanarayanan, M. Soltani, P. Alipour, A. Adibi, *IEEE Photon. Technol. Lett.* 2010, **22**, 1768.
38 D. X. Xu, A. Densmore, A. Delage, P. Waldron, R. McKinnon, S. Janz, J. Lapointe, G. Lopinski, T. Mischki, E. Post, P. Cheben, J. H. Schmid, *Opt. Express* 2008, **16**, 15137.
39 C. Y. Qiu, J. B. Chen, Q. F. Xu, *Opt. Lett.* 2012, **37**, 5012.
40 A. Yariv, *IEEE Photon. Technol. Lett.* 2002, **14**, 483.
41 J. W. Suk, A. Kitt, C. W. Magnuson, Y. F. Hao, S. Ahmed, J. H. An, A. K. Swan, B. B. Goldberg, R. S. Ruoff, *ACS Nano* 2011**, 5**, 6916.
42 M. Prutton, Surface Physics, 2nd ed., Oxford, Clarendon, 1983.
43 U. Fischer, T. Zinke, B. Schuppert, K. Petermann, *Electron Lett.* 1994, **30**, 406.
44 I. N. Kholmanov, C. W. Magnuson, A. E. Aliev, H. Li, B. Zhang, J. W. Suk, L. L. Zhang, E. Peng, S. H. Mousavi, A. B. Khanikaev, R. Piner, G. Shvets, R. S. Ruoff, *Nano Lett.* 2012, **12**, 5679.
45 A. A. Balandin, S. Ghosh, W. Bao, I. Calizo, D. Teweldebrhan, F. Miao, C. N. Lau, *Nano Lett.* 2008, **8**, 902.

Nanoscale Accepted Manuscript